JOURNAL OF CATALYSIS 25, 273–291 (1972)

Aspects of Structure and Activity in U–Sb-Oxide Acrylonitrile Catalysts*

ROBERT K. GRASSELLI AND DEV D. SURESH

The Standard Oil Company (OHIO), Research Department, Cleveland, Ohio 44128

Received October 4, 1971

A uranium–antimony-oxide catalyst, known to be particularly efficient for the synthesis of acrylonitrile, has been studied in order to develop an understanding of structural features related to catalytic activity. The formation of an active and highly selective phase, USb_3O_{10}, of this catalyst and its equally active but less selective precursor, $USbO_5$, were followed by X-ray and low frequency infrared measurements in controlled temperature experiments. Verification of the USb_3O_{10} phase as the catalytically most important was made. Pulse microreactor studies show that there are at least two types of lattice oxygen operative in the reaction. The more labile but less abundant type is mainly involved in the formation of desired products (acrylonitrile and acrolein). Oxygen transfer through the lattice is an important aspect of the oxidation reaction.

A mechanism for the oxidation and ammoxidation of propylene is proposed involving allylic intermediates. The active catalyst site is believed to involve pentavalent antimony, which is stabilized and regenerated through the action of uranium.

INTRODUCTION

Early research in this laboratory on vapor phase oxidation of hydrocarbons was based on the concept that lattice oxygen of reducible metal oxides would serve as a more versatile and functional oxidizing agent than would molecular oxygen (*1*). Using the working hypothesis that metal oxides would be particularly effective if they possessed relatively weak metal–oxygen bonds, crystallographically separated from each other in a structure allowing facile lattice oxygen diffusion, a bismuth phosphomolybdate catalyst (*2, 3*) was discovered among other valuable catalyst systems and was commercialized. It was the most widely used catalyst system for acrylonitrile synthesis from propylene, ammonia, and air. Because of its technical importance in oxidative synthesis, it has been the subject of numerous important investigations and has recently been reviewed (*1*).

* Presented: Int. Symp. Heterogeneous Catalysis, 2nd, Roermond, Netherlands, Jul. 5, 1970.

In 1966, a new, more efficient acrylonitrile catalyst based on a complex U–Sb-oxide system was developed (*4, 5*) and brought into full commercial use. The catalyst was found to consist of discrete phases rather than simple mixtures of oxides (*6*). With the help of several physical methods of analysis, particularly X-ray diffraction, the structures of these phases have been elucidated (*7*).

It is the purpose of this publication to further clarify the relationships between structure and catalytic properties of this commercially significant catalyst.

GENERAL BACKGROUND

Uranium–antimony-oxide catalysts possess high activity and selectivity in both the supported and unsupported form. While acrylonitrile is produced from propylene, ammonia, and air over a wide range of compositions, there is a marked optimum conversion efficiency in the Sb/U range of about 3:1. x-ray diffraction and low frequency infrared analyses clearly demonstrate that two crystalline phases, Phase I (USb_3O_{10}) and Phase II ($USbO_5$), exist in these catalysts and that optimum efficiency for formation of acrylonitrile coincides with the maximum concentration of USb_3O_{10} [Fig. 9, Ref. (*6*)]. Electron spin resonance results show unpaired electrons over the entire range of compositions, thus suggesting the existence of U^{5+} in both crystalline structures. The crystal structure of USb_3O_{10} is orthorhombic belonging to the D_{2h}^{24}-F_{ddd} space group (*7*). The structure of $USbO_5$ is similar to that of USb_3O_{10} except that all atoms are slightly distorted from the basic positions, leading to a lower symmetry subgroup (*7*).

Experimental Methods

Preparation of USb_3O_{10} and $USbO_5$

Method A. USb_3O_{10} and $USbO_5$ can be prepared by starting with Sb_2O_3 and $UO_2(NO_3)_2 \cdot 6H_2O$ and HNO_3 in the respective atomic ratio of 3Sb/1U and 1Sb/1U and heat treating these compositions to 925°C for 16 hr. However, the phases prepared in this manner are not entirely pure; USb_3O_{10} contains a small amount of $USbO_5$ and vice versa [Fig. 4, Ref. (*6*)]. For this reason special preparations of the phases were selected for further studies; comparisons are made below to the conventionally prepared phases where the difference is sufficient for comment.

Method B. Pure USb_3O_{10} was prepared by dissolving the excess antimony oxide with HCl at 100°C from a U–Sb-oxide composition having a high antimony content (U/Sb = 1:9.2) (*6*).

Method C. Pure $USbO_5$ was prepared by thermal decomposition of USb_3O_{10} at 1090°C.

The heavy atom ratio of the compounds was assessed by wet test methods (*8*) and X-ray fluorescence analysis, placing the ratio in Phase I at 3Sb/1U and in Phase II at 1Sb/1U. IEE results (vide infra) support this conclusion.

The oxygen content of the respective phases was determined by an inert gas fusion method (*9*). USb_3O_{10}: theoret, 20.96%; found, 21.09%; $USbO_5$: theoret, 18.19%; found, 18.38%. (Oxygen determinations for the catalysts were carried out by National Spectrographic Laboratories, Inc., Cleveland, OH, using the LECO "Nitrox 6" oxygen analyzer.) TGA results support these formulas, as do the R-factors from the X-ray structure analyses (*7*).

X-ray

X-ray diffraction patterns were obtained on catalyst samples ground to $<44\ \mu$ particle size, using $CuK\alpha$ radiation (λ = 1.5418 Å) and a Ni filter. Each sample was scanned from $2\theta = 7$ to 70° at a rate of 1°/min.

IR

The IR spectra were run on a Perkin-Elmer 521 from 1000 to 250 cm^{-1} or on a Perkin-Elmer 180 from 1000 to 180 cm^{-1}. The wavenumber accuracy is ± 3 cm^{-1} in this region. The samples were examined in CsI pellets after verifying that no changes in spectra occurred due to pelleting. This was done by comparing with Nujol mull spectra taken on identical samples.

Raman

The Raman spectra were recorded on a Spectra Physics Model 700 using a 700 mW Argon ion laser source. The powders were examined directly in capillary melting point tubes. The spectra were recorded from 1000 to 50 cm^{-1}.

IEE

Samples of pure Phase I and II were run by the Varian Analytical Instrument Div., Palo Alto, CA, on their IEE spectrometer. The carbon 1_s line was used as an internal standard for estimating chemical shifts.

Electron Microscopy

a. Transmission. The catalyst samples were studied using a Hitachi 125 E electron microscope with an accelerating voltage of 75 kV and magnifications of 50,000 for the plate and 200,000 for the print.

b. Scanning. The study of the catalyst was carried out at Case Western Reserve Univ. using a Material Analysis Co., Model

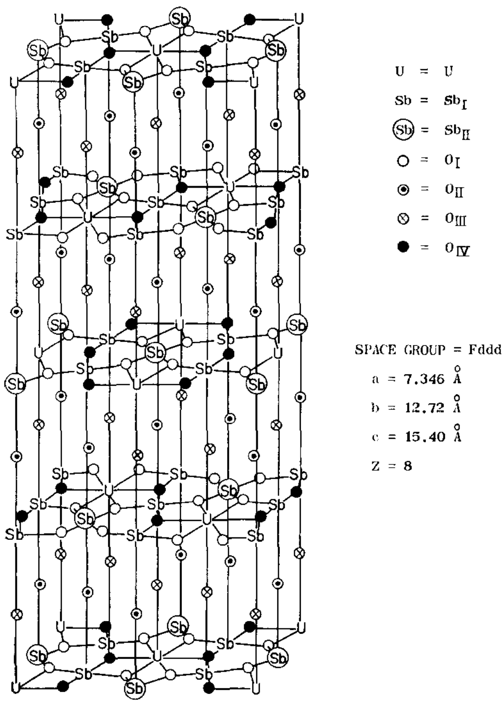

FIG. 1. Unit cell of Phase I (USb_3O_{10}).

700 high resolution scanning microscope having a maximum resolution of 20,000.

DTA

Run on a DuPont Model 900 differential thermal analyzer using a 1200 or 1600°C furnace. Samples were heated at 20°C/min in a purified N_2 atmosphere (air where applicable).

TGA

Run on a Perkin-Elmer TGS-1 at 10 or 20°C/min. 5–10 mg samples were heated in a purified N_2 atmosphere (or air) using a flow rate of 20 ml/min.

RESULTS AND DISCUSSION

A number of spectroscopic tools were utilized to more thoroughly investigate the structures of the two phases for relation to their catalytic efficiency.

The crystal structures were determined from X-ray powder data, since several attempts to prepare single crystals of these phases met with little success. The crystal structure determination has been reported (*7*). The conclusions reached were that USb_3O_{10} contains one type of uranium, two types of antimony and four types of oxygen. The unit cell is composed of eight formula weights ($z = 8$). The 112 atomic positions of this structure are illustrated in Fig. 1. The structure is composed of layers so that those containing heavy atoms and oxygen are alternated by layers of oxygen only. Although the basal plane is hexagonal ($b/a = \sqrt{3}$), the super-

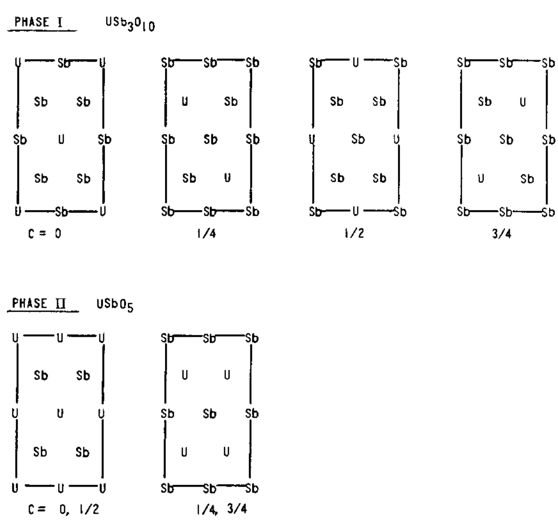

FIG. 2. Heavy atom positions.

FIG. 3A. Transmission electron micrographs: Phase I; 181,250×. B Phase II; 181,250×.

structure is orthorhombic because of glide planes. Five layers of planes containing heavy metal atoms are required to completely describe the unit cell of USb_3O_{10}.

The $USbO_5$ structure is very similar to that of USb_3O_{10}. The conclusion reached from X-ray diffraction (7) suggests that $USbO_5$ has the heavy atoms at positions close to those of USb_3O_{10}, but with a distortion of all atoms, leading to a lower symmetry subgroup. The structures of Phases I and II are therefore closely related to each other (Fig. 2) and to α-UO_3 Kovba and co-workers (*10*) found similar relationships between α-UO_3 and some other mixed uranium oxide systems. In all cases the superstructures are orthorhombic.

FIG. 3B.

Transmission and scanning micrographs of the two phases show that their microcrystalline makeup also appear to be very similar (Figs. 3, 4). Typical particles are about 2000 Å in cross-section and are composed of approximately 10^7 unit cells. These dimensions agree well with those calculated from the density of the pure phases (7) and the surface areas, which range from 1 to 3 m^2/g, depending on the method of preparation. The electron micrographs suggest that the phases grow in the form of platelets.

A normal coordinate analysis is currently underway on both Phases I and II to help with the interpretation of the

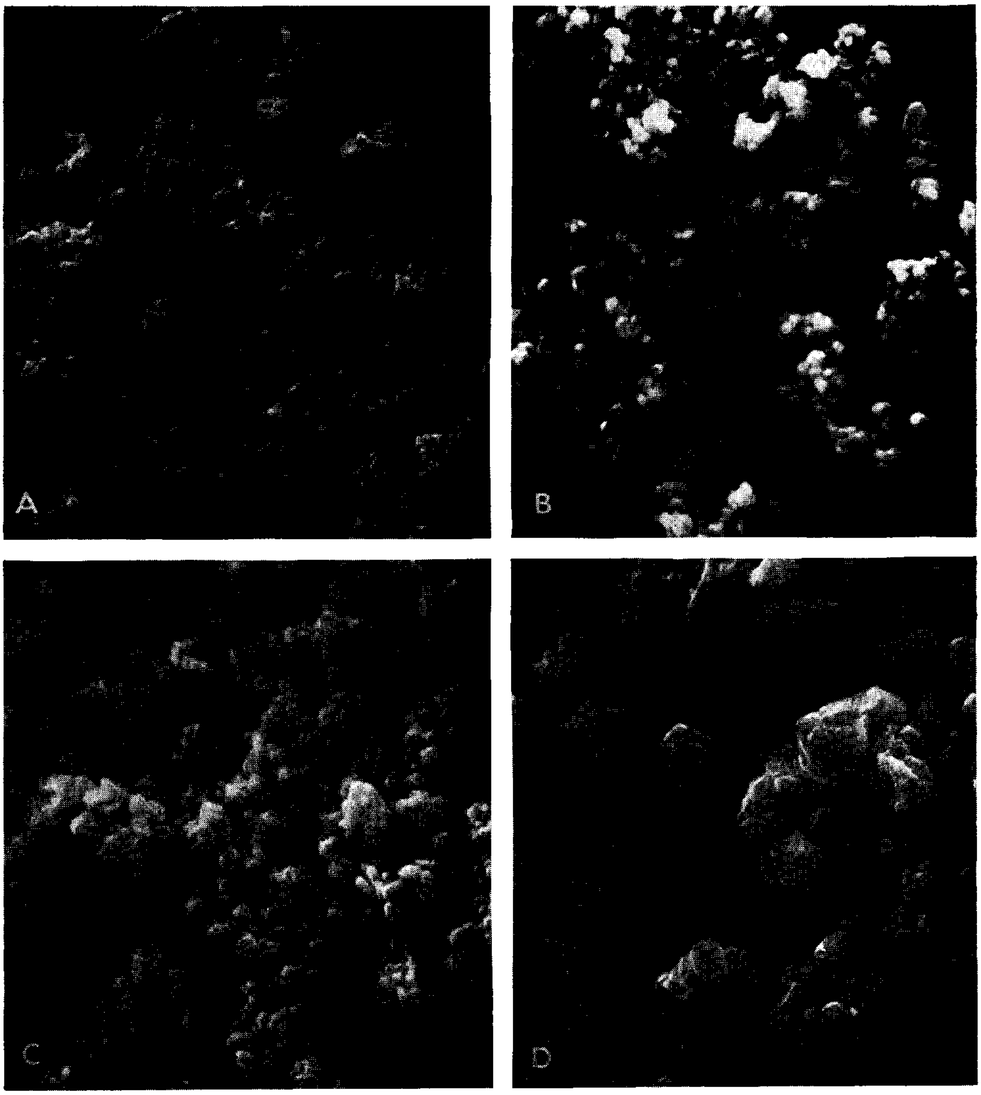

FIG. 4. Scanning electron micrograph: (A) Phase I, 7600×, Method A; (B) phase II, 7600×, Method A; (C) phase I, 7600×, Method B; (D) phase II, 7600×, Method C.

observed infrared and Raman frequencies as related to the crystal structure. Table 1 lists low frequency infrared and Raman bands for both Phases I and II. It is apparent that there are no coincidences of Raman and IR frequencies, which is consistent with the assignment in the point group D_{2h}. Group theoretical analysis predicts 42 Raman and 32 infrared active modes for Phase I, USb_3O_{10}, ($z = 2$) distributed between the symmetry species as shown above.

A_g	7	Raman active
B_{1g}	10	Raman active
B_{2g}	12	Raman active
B_{3g}	13	Raman active
B_{1u}	9	Infrared active
B_{2u}	11	Infrared active
B_{3u}	12	Infrared active
A_u	7	Inactive in Raman and infrared

The unit cell for purposes of normal coordinate calculations of Phase II must be

TABLE 1
LOW FREQUENCY SPECTRA (cm^{-1})[a]

Infrared	Raman	Expected vibrations
A. Phase I	USb_3O_{10}	(prepared by Method A)
930 M		
900 W	910 M	
870 M		Asymmetric + symmetric stretching of $U–O_{III}$, $Sb_I–O_{II}$, $Sb_{II}–O_{II}$
825 SH, M		
	780 S	
730 S	718 W	
702 M		
525 SH	620 VW	
	500 VS	
475 S	475 SH	
460 SH		
435 VVW	450 VW	Asymmetric + symmetric stretching of $U–O_{I,IV}$, $Sb_I–O_I$, $Sb_{II}–O_I$, O_{III}, O_{IV}
430 VVW		
422 W	420 W	
395 SH, VW		
385 SH, W		
375 M		
365 SH, W	360 W	
358 VVW		M–O–M
350 VVW		
335 M		
322 W		
295 M	313 M	
285 M		Bending modes O–M–O
	219 M	
B. Phase II	$USbO_5$	(prepared by Method A)
	902 W	
845 S	830 VW	
780 S		Asymmetric and symmetric stretching of $U–O_{III}$, $U_I–O_{II}$, $Sb–O_{II}$
690 SH, W		
670 SH, M		
630 S	630 VW	
540 W	562 M	
505 SH, VW		
495 SH, W		
478 M	467 M	Asymmetric and symmetric stretching of $U–O_{I,IV}$, $U_I–O_I$, $Sb_{I,III,IV}$, M–O–M
461 SH, VVW		
433 M	447 M	
425 SH		
384 M		
360 S		
331 SH, M	349 S	
305 W		
285 SH, W		Bending modes O–M–O
280 W		

[a] SH = shoulder, S = strong, M = medium, W = weak.

taken as $U_4Sb_4O_{20}$ leading to an identical distribution of frequencies.

The IEE spectra of USb_3O_{10} and $USbO_5$ in the region of the antimony $3d_{3/2}$, $3d_{5/2}$ and uranium $4f_{7/2}$ electrons are shown in Fig. 5. The electron binding energies for the atomic levels of the elements as listed by Siegbahn (*11*) are indicated by arrows. It is significant that only a single line is observed for both elements for the respective electron levels, and that the chemical shifts are comparable for USb_3O_{10} and $USbO_5$. This must be interpreted as strong evidence that only one oxidation state of uranium and one of antimony is present in the compounds. The uranium is in a lower oxidation state than in U_3O_8 (*12*), lending support to the 5+ state indicated by ESR results. Although the Sb $3d_{5/2}$ line is coincidentally overlapped by the O 1*s*, antimony is highly oxidized in the samples. Comparison with Sb_2O_3 (*11*) shows it is higher than 3+, thus 5+ is supported.

A striking difference between the samples is noted in the intensity of the antimony lines which are in a ratio of about 3:1 for Phases I to II, lending further evidence to the correctness of the formulas USb_3O_{10} and $USbO_5$. The uranium lines, on the other hand, are of almost equal intensity in both.

Formation of Phases

Although both phases form simultaneously, Phase II is a precursor of Phase I, which in turn at high temperatures will decompose to Phase II. The mechanism of the active phase formation is visualized to proceed as shown schematically in Fig. 6. The decomposition of the uranyl nitrate and oxidation of the antimony oxide starting materials leads to the formation of UO_3 and Sb_2O_4. The antimony oxide penetrates the lattice of UO_3 in an orderly fashion and forms Phase II over a specified temperature range in a redox reaction:

$$2UO_3 + Sb_2O_4 \rightarrow [2UO_3 \cdot Sb_2O_4] \rightarrow 2USbO_5. \quad (1)$$

A parallel mechanism, shown in Eq. 2, is also suggested by the data:

$$2U_3O_8 + 3Sb_2O_4 + O_2 \rightarrow [6UO_3 \cdot 3Sb_2O_4] \rightarrow 6USbO_5. \quad (2)$$

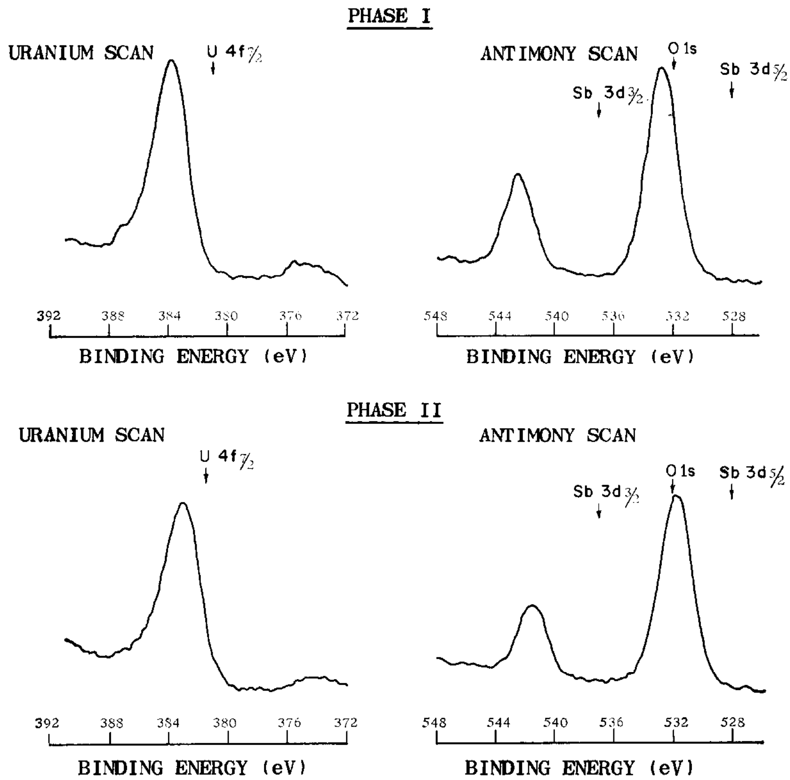

FIG. 5. IEE Spectra of Phases I and II.

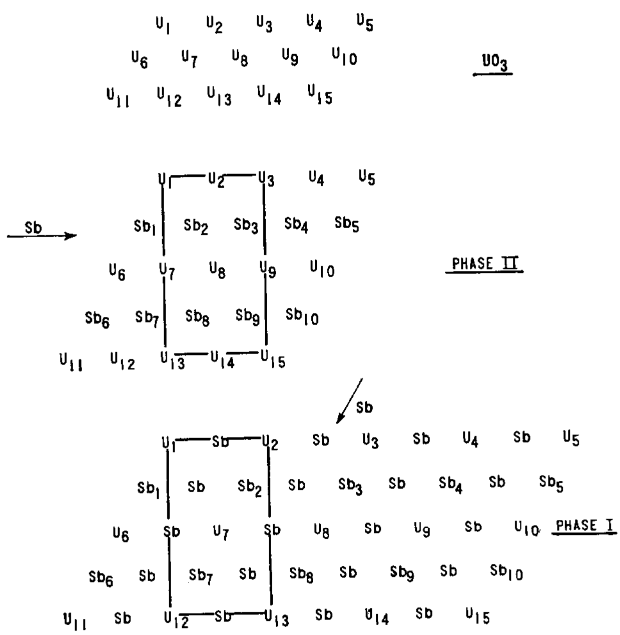

FIG. 6. Schematic of active phase formation.

Subsequently, pentavalent antimony oxide is stabilized by Phase II and can now penetrate the lattice of Phase II again in a very orderly manner but at a higher temperature leading to Phase I:

$$USbO_5 + Sb_2O_5 \rightarrow [USbO_5{\cdot}Sb_2O_5] \rightarrow USb_3O_{10}. \quad (3)$$

The marked crystallographic stabilization of pentavalent antimony oxide by Phase II permits the formation of Phase I even from Sb_2O_4 and gaseous oxygen:

$$USbO_5 + Sb_2O_4 + \tfrac{1}{2}O_2 \rightarrow [USbO_5{\cdot}Sb_2O_5] \rightarrow USb_3O_{10}. \quad (4)$$

The penetration of Sb into the uranium oxide lattice is shown for the basal plane only in Fig. 6. The hexagonal symmetry of all three basal planes is self evident ($b/a = \sqrt{3}$). However, in Phase I hexagonal symmetry holds only for the *ab* planes because in the *c* direction the sheets rearrange (glide planes) as illustrated in Fig. 2.

In order to substantiate the proposed mechanism of formation of the active phase, two series of unsupported U–Sb-oxides in the ratio 1U/3Sb and 1U/1Sb were prepared by Method A and taken through various heat treatments at 50°C intervals. The samples were held for 16 hr at each temperature; and X-ray and low frequency IR were taken at each temperature.

The X-ray results are shown in Figs. 7 and 8. In the 1U/3Sb series, it is seen that Phase II is a precursor of Phase I and forms over the range of about 500 through 900°C, with a low temperature maximum at about 675°C. At this same temperature a maximum concentration of crystalline Sb_2O_5 (or Sb_6O_{13}) is reached. Since Sb_2O_5 and Sb_6O_{13} are not stable at these temperatures by themselves, it is postulated that Phase II stabilizes them. As the temperature is increased, the Sb_2O_5 penetrates the Phase II lattice and Phase I grows until it reaches a maximum concentration at 980°C. Thereafter Phase I becomes temperature unstable and Phase II again forms as O_2 is evolved and Sb_2O_3 is volatilized. A maximum in Phase II is reached at about 1100°C after which it also becomes temperature unstable, losing additional Sb_2O_3 and O_2 and forming high temperature U_3O_8.

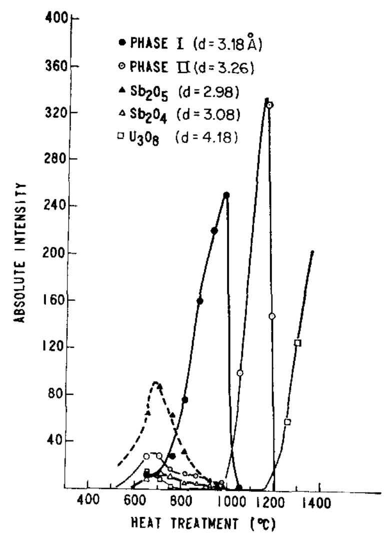

FIG. 7. Compositional makeup of 1U/3Sb oxides as a function of temperature (X-ray).

In an alternate experiment Phase II and Sb_2O_4 were finely ground, mixed in a ratio of $1USbO_5/1Sb_2O_4$, pelleted, and heated to 980°C in air. After 2 hr, over 75% of the crystalline structure, as determined by X-ray, was found to be Phase I.

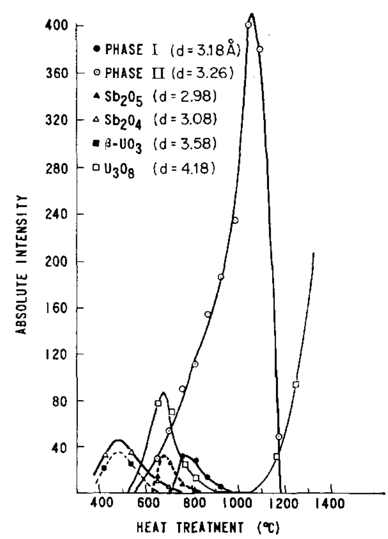

FIG. 8. Compositional makeup of 1U/1Sb oxides as a function of temperature (X-ray).

In the 1U/1Sb series, β-UO_3 and Sb_2O_4 are present until about 600°C at which point Phase II begins to form. Over the range 600 through 800°C, U_3O_8 and Sb_2O_5 are present, both peaking at about 650°C. This suggests that, in addition to the UO_3 + Sb_2O_4 mechanism for the formation of Phase II, there is a parallel mechanism of Phase II formation from U_3O_8 + Sb_2O_5 (or Sb_6O_{13}). A small amount of Phase I is also found over the range 700 through 925°C, peaking at about 790°C. The formation of crystalline Phase II increases steadily starting at 590°C and reaches a maximum at about 1100°C. Above this temperature Phase II becomes temperature unstable, loses Sb_2O_3 and oxygen, and forms high temperature U_3O_8.

The low frequency IR results (Figs. 9 and 10) present a similar picture. The greatest difference between the IR and X-ray results is shown in the Phase II formation. While in the X-ray only one form of Phase II is found, IR finds two forms—a low temperature form and a high temperature form. The low temperature form shows the characteristic 845 cm^{-1} band, but the high temperature form shows this absorption shifted to 800 cm^{-1}. This implies that a slightly different U–O bonding is present in the high temperature form compared to the low temperature form. Most probably, this is a defect structure in the high temperature form. A third, "anomalous" Phase II is also found by IR. It is formed as a transient structure when Phase I is being decomposed to Phase II. This form was isolated during DTA experiments and the characteristic U–O stretch appears now at 870 cm^{-1}. This Phase II is probably Sb rich or has not as yet completely rearranged in the *c* direction from Phase I. All three Phase II's appear identical in the X-ray; therefore significant lattice expansions are ruled out on this basis. However, the subtleness of the IR should be emphasized here (Fig. 11).

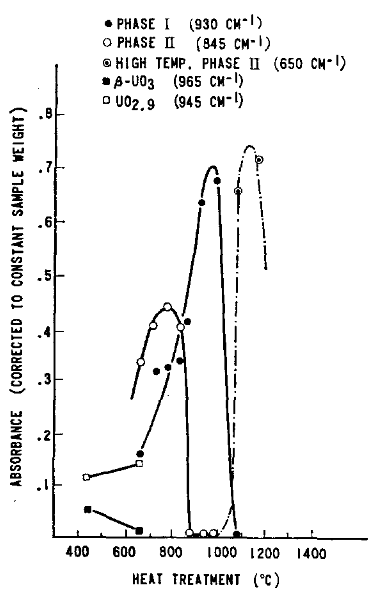

FIG. 9. Compositional makeup of 1U/3Sb oxides as a function of temperature (infrared).

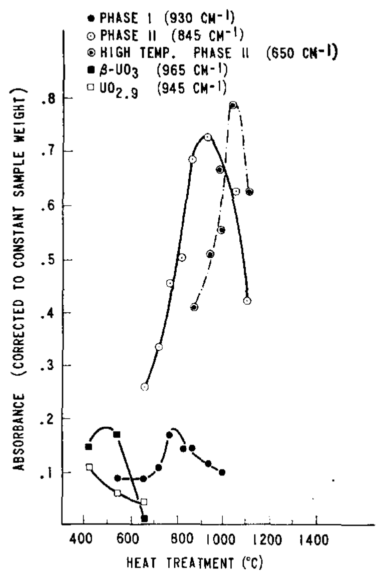

FIG. 10. Compositional makeup of 1U/1Sb oxides as a function of temperature (infrared).

The DTA were also run on unsupported U–Sb-oxides. The results support the conclusions reached above. The decomposition of Phase I to anomalous Phase II is well defined by an endotherm at about 1070°C. Formation of high temperature Phase II from anomalous II occurs endothermically at about 1125°C, and the decomposition of Phase II to U_3O_8 is accompanied by an endotherm at about 1185°C. In air, the

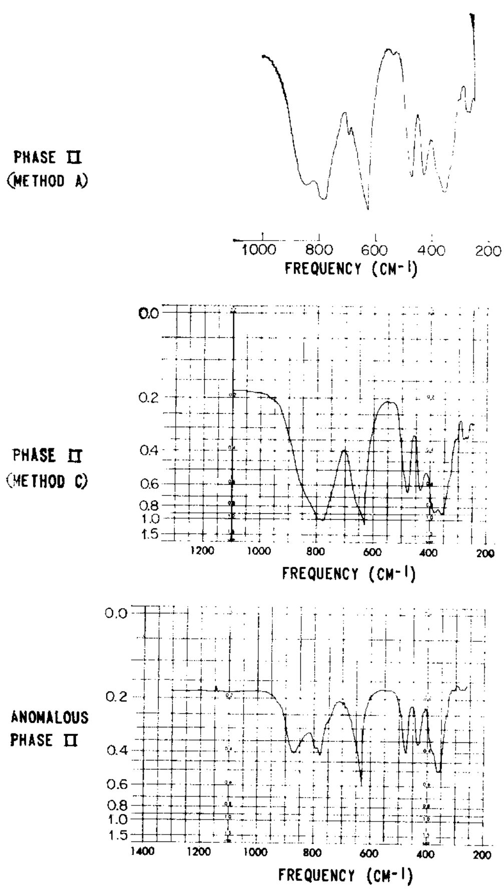

FIG. 11. IR spectra of various Phase II.

decompositions are delayed to 1120, 1155, and 1200°C, respectively (Fig. 12).

Verification of USb_3O_{10} as the Catalytically Effective Component

Phase I and Phase II prepared by Methods A, B, and C (Experimental Section) were examined in 4ml microreactors for the catalytic conversion of propylene to acrylonitrile. The results are summarized in Table 2.

The Phase I prepared by Method B (or what was considered to be pure Phase I) gives the highest acrylonitrile yields over the three temperatures investigated. Phase I prepared by Method A gives somewhat lower results. This is attributed to residual Phase II left in the preparation. Phase II prepared by Method A shows the next lowest acrylonitrile yields and that prepared by Method C shows the lowest yields. It is suggested that some Phase I is left in the Phase II prepared by Method A, thus giving the higher than expected yields.

In order to further establish that Phase I is the most active and selective catalytic specie, an experiment was conducted in which it was attempted to form a surface covering of Phase I on top of Phase II. From the density and surface area of the

TABLE 2

CONVERSION OF C_3H_6 OVER PHASES I AND II PREPARED BY DIFFERENT METHODS

Cat. vol = 4 cm^3; contact time = 5 sec; C_3H_6/NH_3/air = 1:1.2:12.

Catalyst composition	Heat treat. (°C/hr)	Surface area (m^2/g)	React. temp. (°C)	Unreact. C_3H_6	Conversion (mole %) CO_2	CO	Aceto-nitrile	HCN	AN	SEL. to AN
Phase I	925/3	3.7	460	5.4	15.9	1.9	2.1	2.1	72.6	77
USb_3O_{10}			430	21.8	5.5	0.9	3.0	3.5	65.3	84
(Method B)			400	55.1	1.5	1.5	3.1	3.9	34.9	78
(Method A)	925/16	3.2	460	4.8	28.1	2.6	2.1	2.4	62.0	65
			430	11.2	26.9	1.5	2.0	2.4	56.0	63
			400	20.6	21.3	1.0	2.2	2.5	52.4	66
Phase II	925/16	3.2	460	3.0	40.0	6.4	4.1	8.4	38.4	40
$USbO_5$			430	2.6	35.9	3.9	3.1	7.1	47.4	49
(Method A)			400	6.7	30.9	3.1	4.8	6.3	48.2	52
(Method C)	1090/3	1.1	460	29.8	45.5	3.4	2.1	4.8	14.5	24
			430	30.6	42.4	3.5	2.1	4.6	16.8	24
			400	29.0	38.8	2.2	2.8	4.5	22.7	25

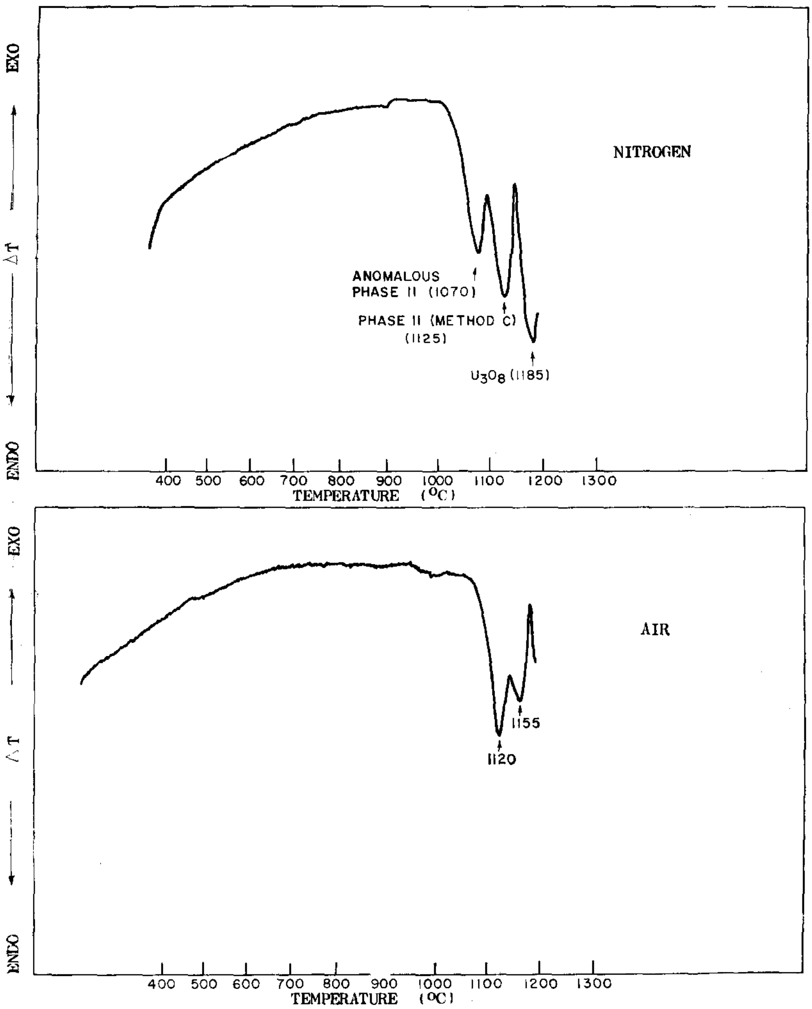

FIG. 12. Differential thermal analysis of Phase I prepared by Method B.

pure Phase II and, independently from the electron microscope data, the amount of Sb_2O_5 needed to give three monolayers of Phase I coverage on top of Phase II was calculated. The empirical formula of such a solid would be $USb_{1.036}O_{5.09}$.

The catalyst was prepared by digesting the pure Phase II with the calculated amount of Sb_2O_3 in the presence of nitric acid. After reflux, neutralization, filtration, and drying at 130°C, the residue was heated in air for 16 hr at 425°C. It was speculated that a 15 min heat treatment at 925°C would be sufficient to form Phase I on the surface of Phase II but would be short enough to prevent the migration of the antimony into the interior of the crystallites. Further, if Phase I can be kept at the surface in this manner, the composition should have catalytic activity very similar to that of pure Phase I but the X-ray diffraction and low frequency IR would see only Phase II. It was postulated that, by heat treating this composition for 3 hr or more at 925°C, the Sb will penetrate into the interior of the crystallites; and the catalytic activity will decrease and ultimately approach that of Phase II. In all cases, the X-ray and IR would still see only the Phase II macro structure.

The catalytic results are shown in Table

TABLE 3
CONVERSION OF C_3H_6 OVER PHASE II AND PHASE II WITH MODIFIED SURFACE
Cat. vol = 4 cm³; contact time = 5 sec; C_3H_6/NH_3/air = 1:1.2:12.

Catalyst composition	Heat treat. (°C/hr)	Surface area (m^2/g)	React. temp. (°C)	Unreact. C_3H_6	Conversion (mole %) CO_2	CO	Aceto-nitrile	HCN	AN	SEL. to AN
$USbO_5$	1090/3	1.1	460	29.8	45.5	3.4	2.1	4.8	14.5	24
$USb_{1.036}O_{5.09}$	925/0.25	1.6	460	2.5	10.3	2.8	1.2	7.0	76.2	78
	925/3	1.0	460	0	33.8	3.7	1.1	7.0	54.4	54
	925/6	1.0	460	1.4	32.2	3.9	0.8	7.2	54.5	55
	925/22	0.9	460	3.6	31.4	4.5	0.9	7.4	52.2	54

3 and bear out the prediction. In further support, X-ray and IR spectra of the $U_1Sb_{1.036}O_{5.09}$ were identical to Phase II.

At this point it was felt that a positive instrumental result would add much to the catalytic evidence. The various samples were run in the infrared using FMIR techniques in the hope of observing the 930 cm^{-1} band, specifically characteristic of Phase I, on the surface of the 15 min 925°C heat-treated sample, but not in the others. The results are shown in Fig. 13. The 930 cm^{-1} band is in fact clearly observed in the catalytically active sample only.

Pulse Microreactor Studies

A pulse microreactor study was carried out at 460°C with a supported catalyst of the composition 70% $USb_{4.6}O_{13.2}$–30% SiO_2 calcined at 925°C. In order to diagnose specific properties of the catalyst, experiments were carried out in the absence of gaseous oxygen; the catalyst functioning as the oxidant.

Propylene, ammonia, and hydrogen all reduce the fully oxidized catalyst which shows conclusively that lattice oxygen can be removed from the catalyst by these reductants. Initial reduction is most severe

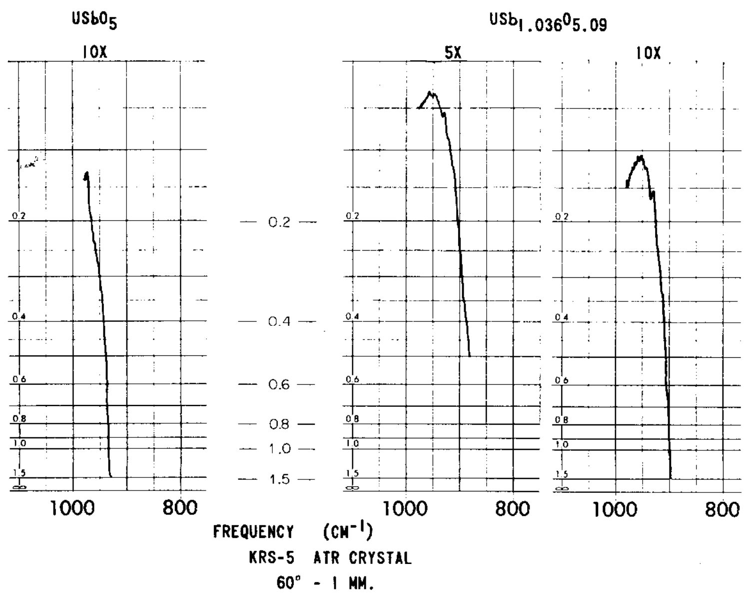

FIG. 13. Ordinate expanded FMIR spectra of $USbO_5$ and $USb_{1.036}O_{5.09}$.

with propylene, followed by H_2 and NH_3. On deep reduction however, propylene becomes the mildest reductant, followed by NH_3 and H_2.

The test reaction chosen to determine the amount and distribution of the useful lattice oxygen was the oxidation of propylene to acrolein. Using propylene as a reductant, the formation of acrolein is highest with the fully oxidized catalyst and drops off sharply with catalyst reduction (Fig. 14). Conversion to waste products (CO_2 and CO) is low when the catalyst is fully oxidized and decreases with reduction; yet waste production becomes the prevalent reaction as reduction is carried on further. The formation of acrolein ceases when 6.5% of the lattice oxygen is removed from the catalyst. (The calculation is based on USb_3O_{10} reducing to USb_3O_9.)

Useful information about the catalyst behavior as a function of its oxidation state can be secured by pre-reducing a catalyst with reductants such as propylene, NH_3, or H_2, followed by a measured pulse of propylene. Ammonia is a convenient pre-reductant since it is very mild; and therefore catalyst oxidation states very close to fully oxidized can readily be attained. However, it is immaterial whether propylene, ammonia, or hydrogen is used for *pre*-reduction, the formation of acrolein from propylene through lattice oxygen abstraction is a function only of the catalyst oxidation state. Acrolein formation decreases with increasing reduction of the catalyst and again ceases once 6.5% of the lattice oxygen is removed (Fig. 15).

In another set of experiments, the catalyst was separately reduced to various levels by propylene, NH_3, and H_2. After each reduction the level of the reduction was determined by back titration with gaseous oxygen which was followed by exposure to a stream of gaseous oxygen for 15 min at reaction temperature (i.e., 460°C). Following the reoxidation a stream of helium was passed over the catalyst for 15 min to remove gaseous oxygen from the reactor. Then a constant volume pulse of propylene was passed over the catalyst; and the formation of acrolein was monitored (Fig. 16). An amount of acrolein is formed under these conditions with a catalyst which has not been reduced beyond 6.5% which is identical to that formed over a fully oxidized catalyst. This is exactly the same quantity obtained above in an entirely different way.

These results suggest that there are at least two types of lattice oxygen involved in the oxidation and ammoxidation reactions. One type of oxygen (A-type) is primarily involved in producing useful products (i.e., acrolein or acrylonitrile) while another type of lattice oxygen (B-type) is primarily involved in producing waste products (i.e., CO_2 + CO). Further,

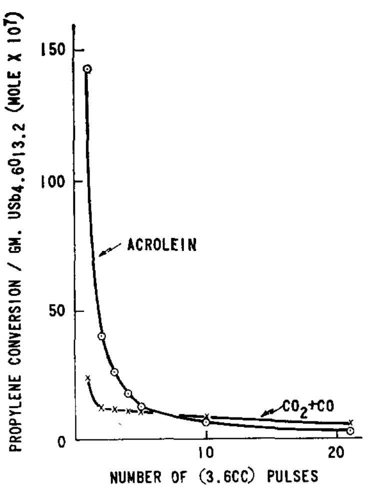

FIG. 14. Acrolein production as a function of propylene pulses (catalyst reduction).

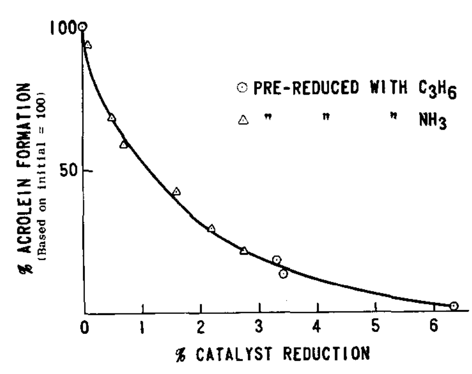

FIG. 15. Activity of 70% $USb_{4.6}O_{13.2}$–30% SiO_2 as a function of its oxidation state (460°C).

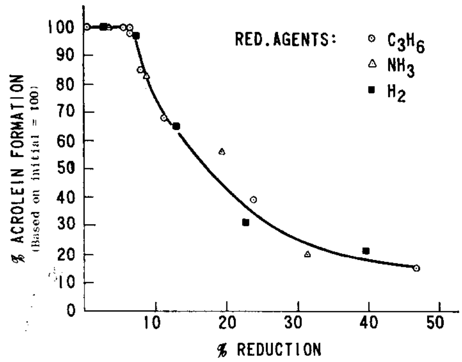

FIG. 16. Activity of 70% $USb_{4.6}O_{13.2}$–30% SiO_2 as a function of its reduction history (460°C).

it can be concluded that the number of A-type oxygens (6.5% of total) is much smaller than that of the B-type oxygens, and that the reactivity of the A-type oxygens is much higher than that of the B-type oxygens, which are probably more tightly bound. Assuming pseudo-second order reactions, the rate constants for the removal of the two types of oxygen by propylene, ammonia, or hydrogen can be calculated and are given in Table 4.

Another conclusion is that once all of the A-type oxygen is removed from the lattice of USb_3O_{10} it becomes difficult to replenish it. However, all of the more severely reduced catalysts can be brought back to their original useful activity. Those reduced to between 6.5 and 30% can readily be brought back to the normal activity by air regeneration at 460°C. Catalysts reduced to levels between 30 and 100% must be heated in air at a temperature above 460°C. From a practical standpoint for both ammoxidation and oxidation

TABLE 4
PSEUDO-SECOND ORDER RATE CONSTANTS FOR THE REMOVAL OF OXYGEN FROM 70% $USb_{4.6}O_{13.2}$–30% SiO_2 AT 460°C (catalyst reduction)

	k (g atoms^{-1} sec^{-1}/gm $USb_{4.6}O_{13.2}$)	
Reductant	Type-A oxygen	Type-B oxygen
C_3H_6	3.3×10^3	1.2×10^{-1}
NH_3	1.2×10^2	6.3×10^{-1}
H_2	—	2.3

reactions, it is advisable to maintain the catalyst in a high oxidation state.

If it is assumed that one oxygen per USb_3O_{10} formula weight is a useful oxygen, then from density and surface area measurements of the active component, one can estimate that type-A oxygen can move to the surface from the interior of the catalyst and that as many as 70 atomic layers can be involved. It is however, also possible that type-A oxygen of the complete crystallite of USb_3O_{10} participates in the useful oxidation. If this is the case, then within the crystallite 0.65% of the total oxygen is type-A, which can transfer readily throughout the entire lattice.

Crystallographically it is plausible to assign type-A oxygen to O_{IV} of Phase I and type-B to O_I of Phase I.

Experiments with Deuterated Propylenes

Various deuterated propylenes were oxidized and ammoxidized over a 70% $USb_{4.6}O_{13.2}$–30% SiO_2 catalyst and the respective products analyzed by MS and IR techniques. The results are summarized in Table 5.

The conclusion drawn from these results is that propylene proceeds over an allylic intermediate after the abstraction of the first α-hydrogen and that the first α-hydrogen abstraction is the rate-limiting step. This step is followed by a second hydrogen abstraction from either end of the allylic intermediate. From this stage on, the oxidative reaction proceeds to the final product acrolein or acrylonitrile, depending upon whether ammonia is absent or present in the feed. This part of the mechanism is less well understood.

These results are in essential agreement with those found by Adams and Jennings (*13*, *14*) and by Sachtler (*15*) and Sachtler and DeBoer (*15*, *16*) using a Bi–Mo-oxide catalyst.

Probable Mechanism of Propylene Reaction

Experimental evidence points to the necessity of having Sb^{5+} in an octahedral environment for the useful oxidation or ammoxidation of propylene with U–Sb-

TABLE 5

RESULTS WITH DEUTERATED PROPYLENES IN OXIDATION AND AMMOXIDATION STUDY

Catalyst, 70% $USb_{4.6}O_{13.2}$-30% SiO_2; temp, 460°C.

Starting material	Products	Experimental		Theoretical-allylic intermed.
		M.S.	IR	
	Oxidation			
$CD_3CH{=}CH_2$ (94%)	$CD_2{=}CHCHO$	62.5	64	63.6
(6% dideut. $C_3^=$)	$CH_2{=}CHCDO$[a]	33.3	32	35.7
	$CH_2{=}CHCHO$	4.2	4	0.7
$CH_3CH{=}CD_2$ (87%)	$CD_2{=}CHCHO$	56.0	59	56.8
(13% monodeut. $C_3^=$)	$CH_2{=}CHCDO$	36.4	39	41.1
	$CH_2{=}CHCHO$	7.7	2	2.1
$CH_3CD{=}CH_2$ (93%)	$CH_2{=}CDCHO$	92.0	93	93
(7% undeut. $C_3^=$)	$CH_2{=}CHCHO$	8.0	7	7
	Ammoxidation			
$CD_3CH{=}CH_2$ (94%)	$CD_2{=}CHCN$	63.1	65	63.6
(6% dideut. $C_3^=$)	$CDH{=}CHCN$	34.9	31	33.8
	$CH_2{=}CHCN$	2.0	4	2.6
$CH_3CH{=}CD_2$ (87%)	$CD_2{=}CHCN$	56.2	58	56.8
(13% monodeut. $C_3^=$)	$CDH{=}CHCN$	38.3	36	34.7
	$CH_2{=}CHCN$	5.5	6	8.5
$CH_3CD{=}CH_2$ (93%)	$CH_2{=}CDCN$	92.2	93	93
(7% undeut. $C_3^=$)	$CH_2{=}CHCN$	7.8	7	7

[a] Some $CDH{=}CHCHO$ also present.

oxide catalysts. Antimony oxides by themselves are unreactive but quite selective and uranium oxides by themselves are strong waste formers. It appears reasonable that the uranium in Phases I and II stabilizes the Sb^{5+} state. In addition to stabilizing Sb^{5+} by structural means, uranium also provides a path via a redox reaction for its reformation once it has been reduced to a lower oxidation state in the course of the propylene oxidation or ammoxidation reaction.

A mechanism for propylene oxidation and ammoxidation over U–Sb-oxide catalysts which emerges from these considerations is shown in Fig. 17. This scheme is consistent with the experimental findings and in some respects is similar to the oxidation mechanism proposed by Schuit and co-workers (*17*) and by Trifiro and co-workers (*18*) for the Bi–Mo-oxide system. It is envisioned that propylene chemisorbs on an active site of Phase I (USb_3O_{10}) which can be written as:

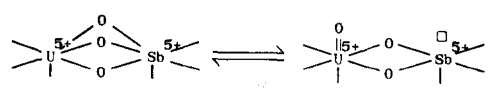

The U^{5+} might be replaced by Sb^{5+} on the surface of the active phase provided it is bonded through oxygen to U^{5+} in the underlying layer. As the propylene is chemisorbed at the antimony vacancy, it loses an α-hydrogen to a uranyl oxygen. It is uncertain as to whether this hydrogen is lost as a proton or a radical. For purposes of electron accounting we can assume it is lost as a proton. The addition of a proton to a uranyl oxygen results in a uranium atom with a formal charge of U^{6+}. The coordination of the Π-allyl residue to Sb results in the reduction of Sb^{5+} to a formal oxidation state of Sb^{4+}. The resulting complex is shown in the figure. The U^{6+} and Sb^{4+} can then disproportionate to produce the two metal atoms in the equal oxidation state of 5+.

The Π-allylic moiety is planar and

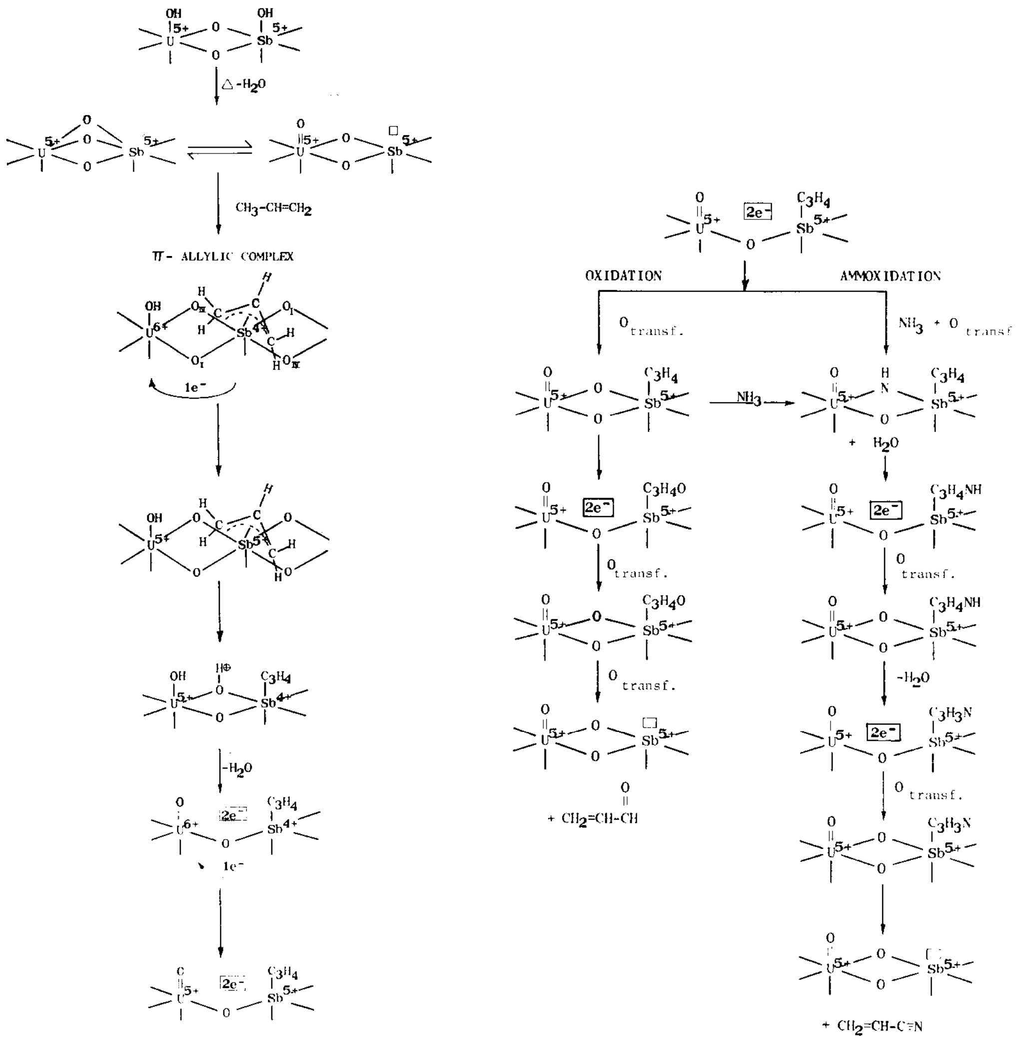

FIG. 17. Probable mechanism of propylene oxidation and ammoxidation.

parallel to the surface of the catalyst and finds equivalent lattice oxygen atoms about the Sb atom to which it is attached. Two O_{IV} atoms are positioned at opposite corners of the distorted octahedron around Sb as shown.

The next step involves a second hydrogen abstraction. Since O_{IV} is crystallographically the most loosely held, it is assumed that the second hydrogen is abstracted by one of these oxygens from either of the equivalent terminal methylenes of the first allylic complex. Although we have no direct evidence for the structure of the highly hydrogen deficient C_3H_4 moiety (but whose presence is inferred from the isotope kinetic studies) its stoichiometry is consistent with a vinyl carbene, $CH_2{=}CH{-}CH{:}$. In any case, loss of water from the new complex follows, creating an anion vacancy in the immediate vicinity of this complex after some electron rearrangement. This anion vacancy can be readily filled with an oxygen from the underlying layers by rapid lattice oxygen transfer.

Depending on whether or not NH_3 is present at this stage, the C_3H_4 complex can react further to give either acrolein or acrylonitrile. The probable paths are shown in Fig. 17. In the absence of NH_3, the oxygen inserts into the C_3H_4 complex and after electronic rearrangement forms chemisorbed acrolein which desorbs and the site is regenerated. In the presence of ammonia, the lattice oxygen reacts with NH_3, forming an NH which inserts into the C_3H_4 complex as shown. It is known that acrolein is not a major isolatable intermediate in the ammoxidation of propylene to acrylonitrile either over Bi–Mo-oxide (*1*, *19*), or U–Sb-oxide catalysts.

It is believed from this study that the oxygens involved in the reaction reach the active sites primarily by means of lattice oxygen transfer. Gaseous oxygen is incorporated into the crystal lattice through other regeneration sites and from these the lattice oxygens are transfered to the active sites. This view is supported by relaxation experiments, O_{18} exchange work, and by analogy to the Bi–Mo-oxide system (*20–22*).

Conclusions

The interrelationship between structure and catalytic behavior is clearly a complex one in the U–Sb-oxide system. However, this investigation was purposely aimed at attempting to bring a measure of understanding to the function of this catalyst. A multitude of physical and chemical tools were brought to bear on the problem; and all contributed to the final conclusions.

In the course of the investigation, it was discovered that distinctive phases of fixed chemical composition are present in the catalysts as opposed to simple mixtures of oxides. USb_3O_{10} (Phase I) and $USbO_5$ (Phase II) were identified, characterized, and their crystal structure was determined. Both phases were prepared in nearly pure form and were catalytically active. Phase I is the more selective and efficient phase for the formation of acrylonitrile from propylene, ammonia, and oxygen. This was demonstrated by testing the activity of a composition with only a surface covering of Phase I on Phase II.

A mechanism for formation of the active phases was suggested, and the domain of their existence was defined by taking known chemical compositions through an extensive temperature study and identifying the resultant structures by X-ray and low frequency infrared.

Based on the structure of the phases it is concluded that there is one type of uranium, two types of antimony, and four types of oxygen in Phase I. In Phase II there are two types of uranium, one type of antimony, and four types of oxygen. It is believed that at least two types of the oxygens participate in the oxidation and ammoxidation reaction. The more labile but less abundant oxygen (probably O_{IV}) leads to useful products while the more populous but more tightly bound oxygen (probably O_I) leads to waste products. Oxygen transfer through the lattice of the active phases is an important aspect of useful catalysis.

The mechanism of propylene oxidation and ammoxidation proceeds by the abstraction of an α-hydrogen after the propylene has chemisorbed on the surface and the rate is controlled by this step. Experiments with deuterated propylene show that the mechanism on U–Sb-oxides is similar to that previously shown to be operative on Bi–Mo-oxide catalysts. The adsorption site is, however, postulated to be an oxygen ion vacancy on Sb^{5+}. The uranium is postulated to be important in stabilizing Sb^{5+} structurally and in aiding its regeneration with gaseous oxygen during the course of catalytic operation.

Acknowledgments

The authors gratefully acknowledge the many fruitful discussions with Dr. J. L. Callahan pertaining to this work, and his continued encouragement. Appreciation is also expressed for the contributions of M. S. Friedrich, R. A. Gerron, J. G. Grasselli, M. A. Hazle, L. E. Wolfram, and Professor Milton Orchin (Univ. of Cincinnati).

References

1. Callahan, J. L., Grasselli, R. K., Milberger, E. C., and Strecker, H. A., *Ind. Eng. Chem. Prod. Res. Develop.* **9**, 134 (1970).

2. IDOL, J. D., JR. (Standard Oil Co.), *U. S. Pat.* 2,904,580 (Sept. 15, 1959).
3. CALLAHAN, J. L., FOREMAN, R. W., AND VEATCH, F. (Standard Oil Co.), *U. S. Pat.* 3,044,966 (Jul. 17, 1962).
4. CALLAHAN, J. L., AND GERTISSER, B. (Standard Oil Co.), *U. S. Pat.* 3,198,750 (Aug. 3, 1965).
5. CALLAHAN, J. L., AND GERTISSER, B. (Standard Oil Co.), *U. S. Pat.* 3,308,151 (Mar. 7, 1967).
6. GRASSELLI, R. K., AND CALLAHAN, J. L., *J. Catal.* **14**, 93 (1969).
7. GRASSELLI, R. K., SURESH, D. D., AND KNOX, K., *J. Catal.* **18**, 356 (1970).
8. (a) BOOMAN, G. L., MAECK, W. J., ELLIOT, M. C., AND REIN, J. E., *Anal. Chem.* **31**, 1130 (1959). (b) ELKIN, A., GAYER, K. H., AND BOLTZ, D. F., *Anal. Chem.* **25**, 1744 (1953).
9. SMITH, S. K., AND KRAUSE, D. W., *Anal. Chem.* **40**, 2034 (1968).
10. KOVBA, L. M., SIROTKINA, E. I., AND TRUNOV, V. K., *J. Neorg. Khim. SSSR* **10**, 349 (1965).
11. SIEGBAHN, K., "Electron Spectroscopy for Chemical Analysis," Technical Report AFML-TR-68-189 (Oct., 1968).
12. HULETT, L. D., AND CARLSON, T. A., private communication.
13. ADAMS, C. R., AND JENNINGS, T. J., *J. Catal.* **2**, 63 (1963).
14. ADAMS, C. R., AND JENNINGS, T. J., *J. Catal.* **3**, 549 (1964).
15. SACHTLER, W. M. H., *Recl. Trav. Chim. Pays-Bas* **82**, 243 (1963).
16. SACHTLER, W. M. H., AND DEBOER, H. H., *Proc. Int. Congr. Catal., 3rd 1964,* **1**, 252 (1965).
17. BATIST, P. A., KAPTEIJNS, C. J., LIPPENS, B. C., AND SCHUIT, G. C. A., *J. Catal.* **7**, 33 (1967).
18. TRIFIRO, F., KUBELKOVA, L., AND PASQUON, I., *J. Catal.* **19**, 121 (1970).
19. CATHALA, M., AND GERMAIN, J. E., *Bull. Soc. Fr.* **11**, 4114 (1970).
20. SCHUIT, G. C. A., *Chim. Ind. (Milan)* **51**, 1307 (1969).
21. KEULKS, G. W., *J. Catal.* **19**, 232 (1970).
22. HOCKEY, J. A., *Int. Symp. Het. Catal., 2nd,* Roermond, Netherlands, Pap. No. 2 (1970).